Low-Profile MIMO Antenna Arrays with Left-Handed Metamaterial Structures for Multiband Operation

Ayman Ayd R. Saad*

Abstract—In this article, a design of two low-profile multiple-input-multiple-output (MIMO) antenna arrays based on left-handed metamaterial (LHM) structures is proposed for multiband wireless applications. The single-element antenna is a monopole antenna fed by a microstrip transmission-line loaded with a single LHM unit cell. The LHM unit cell structure consists of a right-angled bend interdigital capacitor and dual symmetrical right-angled bend shorted stub inductors. The loaded monopole antenna was previously designed to operate in the left-handed (LH) frequency region at three negative-order resonance modes (i.e., 1.39, 1.88, and 2.35 GHz). Herein, to increase the designed antenna performance in wireless communication systems, two- and four-element MIMO antenna arrays having compact sizes with overall dimensions of $21 \times 35\,\text{mm}^2$ and $35 \times 35\,\text{mm}^2$, respectively, are realized. A close uniform edge-to-edge separation between antenna elements of each configuration equals only $2\,\text{mm}$ $(0.0093\lambda_0$ at $1.39\,\text{GHz})$, and port isolation more than $18\,\text{dB}$ over the entire operating bands is obtained without using extra isolation structures. Envelope correlation coefficient is evaluated, showing good field isolation. The performance of the assembled MIMO antenna arrays is verified numerically and experimentally. The given attributes make the proposed antenna arrays a suitable candidate for multiband MIMO applications.

1. INTRODUCTION

In modern wireless communication systems, the growing search for higher data rate and higher channel capacity without the necessity to increase the spectrum bandwidth and transmit power has led to the use of several antennas at both exciting and receiving sides, such a technique called multiple-input-multiple-output (MIMO) antenna system, which has a major impact on increasing the performance of such systems [1]. However, in modern portable devices, a limited area is dedicated to antennas required for different applications; therefore, for MIMO applications, several antenna elements should be placed in close proximity to each other, which may lead to performance degradation because of mutual electromagnetic (EM) interactions between the adjacent edges of antenna elements, known as mutual coupling.

Mutual coupling can greatly influence the isolation as well correlation of neighbored antenna elements. Therefore, high port isolation and low field correlation are both required to ensure high MIMO antenna system performance. Port isolation is evaluated using transmission coefficient, while field correlation is evaluated using envelope correlation coefficient (ECC) of the antenna system [2]. In this context, several techniques have been introduced in literature to suppress the mutual coupling effect and ensure efficient operation [3]. The simplest and most effective techniques include the use of parasitic elements or slots [4, 5], decoupling networks [6, 7], neutralization lines [8], electromagnetic band-gap (EBG) structures [9], defected ground structures (DGSs) [10], and orthogonal asymmetric

feeding schemes [11, 12]. These techniques can suppress the mutual coupling by reducing the surface current flow.

In recent years, metamaterials have been widely exploited to design MIMO antenna systems with low mutual coupling between radiating elements [13–18]. This comes from the ability of such structures to distribute fields near antenna structures, rather than diffusing them along the ground plane. In general, metamaterials can be described as a mixture of left-handed (LH) materials and right-handed (RH) materials, and thus they are commonly known as composite right/left-handed (CRLH) metamaterials. At low frequencies, a CRLH metamaterial acts like an LH material, while at high frequencies it acts like an RH material. Such structures can be implemented by loading microstrip transmission lines with series capacitive and shunt inductive loads [19].

In open literature, many researchers have used CRLH metamaterials to design different planar antennas geometries, characterised by miniaturized structures and multifunctionality operation [20–31]. These designs depend on the unique feature of metamaterials of exhibiting zero or negative progressive phase values at arbitrary frequencies, which allow antennas to resonate at zeroth-order mode ($n = 0$) or negative-order modes ($n = -1, -2, \ldots$), respectively [19].

In this work, two compact MIMO antenna arrays based on LHM structures are proposed for multiband operation. The assembled MIMO antenna arrays have two and four elements, based on previously developed LHM unit cell by the author. The antennas' design was accomplished to operate at three narrow bands in the LH frequency region, covering Wireless Medical Telemetry Service, WMTS (1.395–1.40 GHz), Digital Enhanced Cordless Telecommunications, DECT (1.88–1.90 GHz), and Wireless Communications Service, WCS (2.345–2.360 GHz) standards, while the port isolation is more than 18 dB over the entire operating frequency bands with only 2 mm physical spacing between antennas elements edges. In the two MIMO structures, antennas elements were etched on low-profile printed circuit boards (PCBs) to ensure easy integration within mobile platforms. The antennas designs were verified by the good agreement of the three dimensional (3D) electromagnetic (EM) simulation results performed using CST$^{\textregistered}$ Microwave Studio with the measured data of implemented models.

2. MULTIBAND LHM MIMO ANTENNA ARRAYS DESIGN

The geometrical configurations of the proposed LHM MIMO antenna arrays are pictured in Figure 1, with a descriptive caption for design parameters. The antennas are built on FR-4 substrates having relative permittivity, loss tangent, and thickness of 4.3, 0.025, and 1.524 mm, respectively. The single-element antenna which was previously designed by the author is used as a basis to design the proposed MIMO antenna configurations [32]. As the former study, the single-element antenna is a monopole antenna fed by a microstrip transmission line loaded with an open-ended LH unit cell formed of a series interdigital capacitor (IDC) and dual shorted shunt stub inductors. The right-angled microstrip bend technique was utilized in the design of the unit cell to achieve high level of miniaturization [32]. The first (initial) MIMO antenna array configuration has two identical radiating elements arranged in parallel orientation side by side with uniform separation equal to only 2 mm, while the second MIMO antenna array configuration has four elements and is realized by adding two more elements to the opposite side of the ground plane with the same separation distance of 2 mm, which is chosen via parametric study. In such a configuration, antenna elements 1 & 2 and 3 & 4 are seen to be side by side, whereas antenna elements 1 & 4 and 2 & 3 are seen in across orientation with respect to each other (see Figure 1(b)). The two- and four-element MIMO antenna arrays having compact sizes with overall dimensions of $21 \times 35 \, \text{mm}^2$ and $35 \times 35 \, \text{mm}^2$, respectively.

The simulated S-parameters behaviors of the proposed two- and four-element LHM MIMO antenna arrays are shown in Figures 2(a) and 2(b), respectively. Results show that the two antenna configurations achieve typical three narrow frequency bands in the LH frequency region centered at 1.39 ($n = -3$), 1.88 GHz ($n = -2$), and 2.35 GHz ($n = -1$). The 10 dB impedance bandwidth of the first band is 20 MHz (1.38–1.40 GHz, 1.44%); the second band is 40 MHz (1.86–1.90 GHz, 2.13%); and the third band is 40 MHz (2.33–2.37 GHz, 1.70%). Also, results in Figure 2 show that the designed MIMO antenna array with the two configurations maintains a minimum isolation of 18 dB in the entire covered operating bands in which they were configured to be mirror of each other so that the current can be reversed, resulting in reduction of the mutual coupling between them. The uniform edge-to-edge
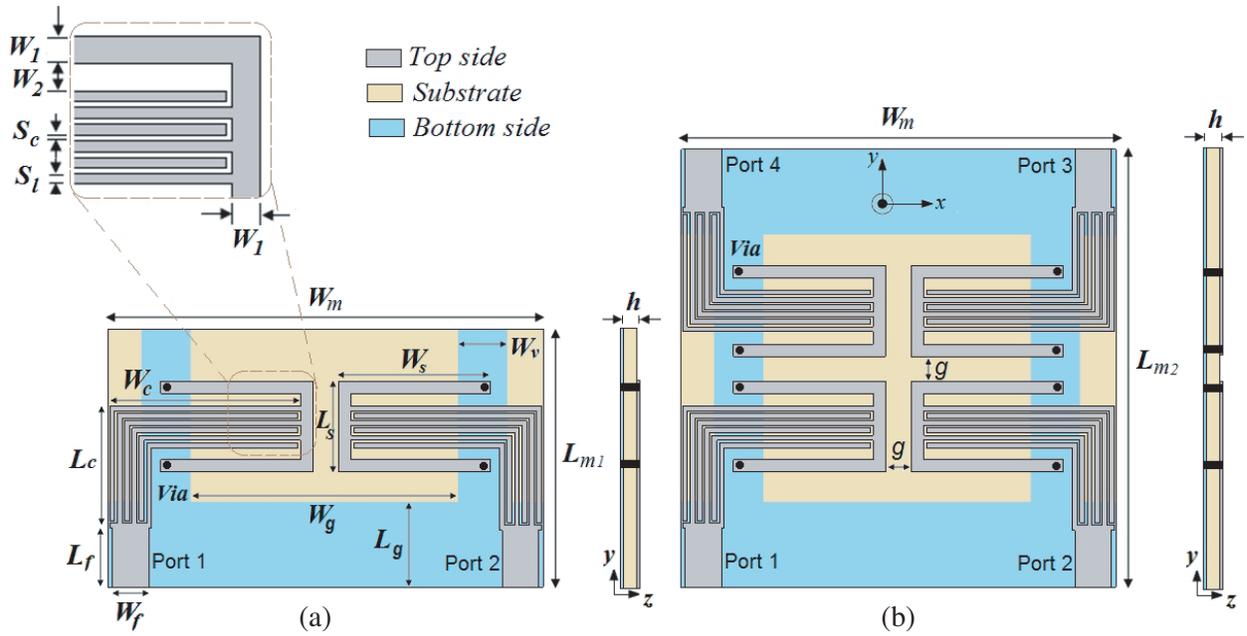
Figure 1. Geometrical configurations of the proposed multiband LHM MIMO antenna arrays. (a) Two-element configuration and (b) four-element configuration. $L_{m1} = 21$ mm, $L_{m2} = 35$ mm, $W_m = 35$ mm, $L_f = 5$ mm, $W_f = 3$ mm, $L_c = 10$ mm, $W_c = 15.5$ mm, $L_s = 7.4$ mm, $W_s = 12.4$ mm, $L_g = 7$ mm, $W_g = 21$ mm, $W_v = 4$ mm, $W_1 = W_2 = 1$ mm, $S_c = 0.2$ mm, $S_l = 0.4$ mm, $g = 2$ mm, $h = 1.524$ mm.
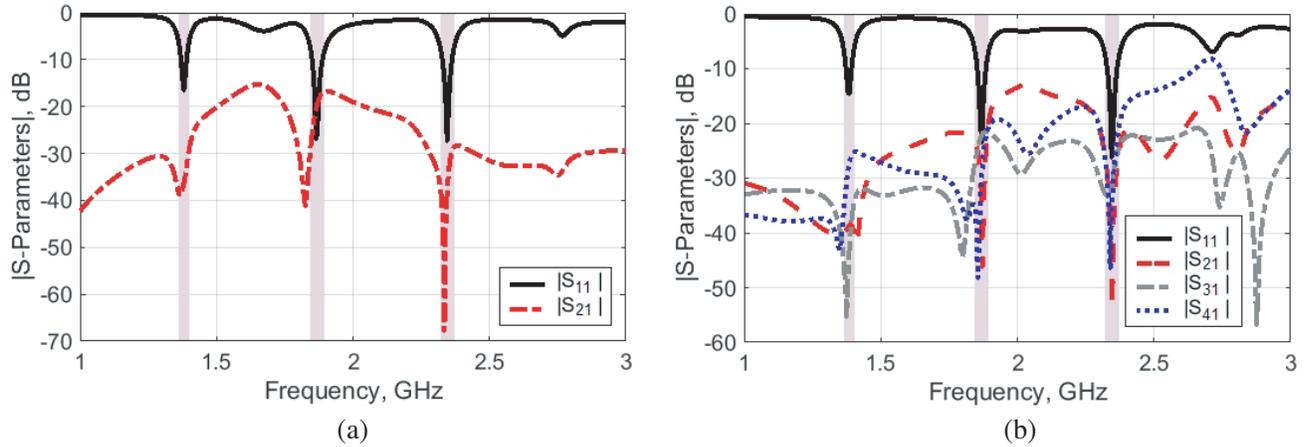
Figure 2. Simulated S-parameters versus frequency of the proposed LHM MIMO antenna arrays. (a) Two-element configuration and (b) four-element configuration.

separation between antennas elements equals $0.0093\lambda_0$ at 1.39 GHz.

To further understand the isolation mechanism, simulated current distributions at the different resonant frequencies of 1.39, 1.88, and 2.35 GHz of the comprehensive design of four-element LHM MIMO antenna array when port 1 is activated and other ports matched with 50 Ω loads are depicted in Figure 3. For the sake of simple illustration, current density scales of the three plots were unified. From the figure, it is obvious that the current is concentrated in the series IDC, while small current is distributed along the shorted dual symmetric shunt stubs, which indicates that the IDC is the main radiator of the antenna. Also, it is obvious that the mirror configuration of the IDC elements caused in coupling a small amount of current from the activated port to other ports, which can lead to high
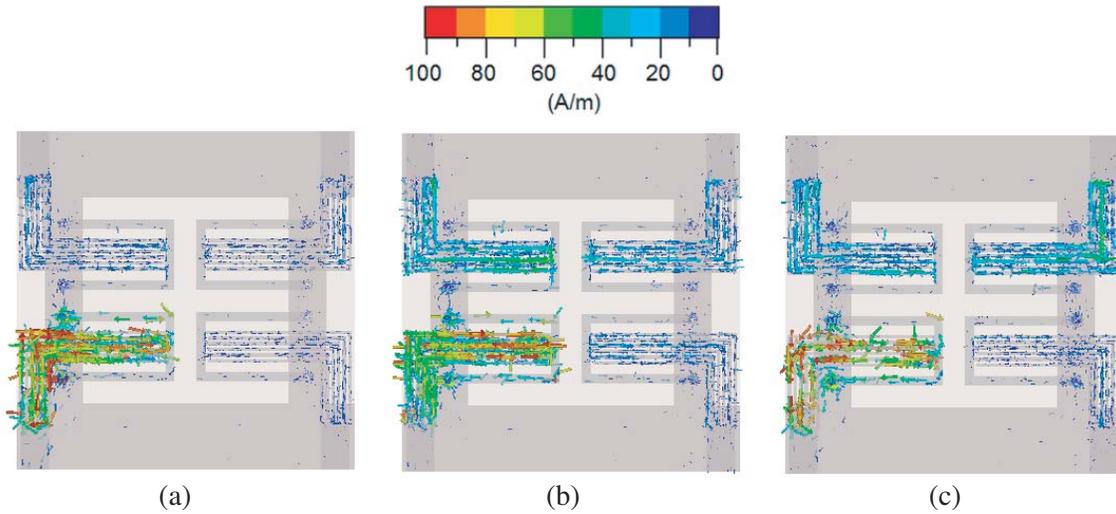
Figure 3. Simulated surface current distributions of the proposed four-element LHM MIMO antenna array when port 1 is activated at the three LH resonant frequencies (a) 1.39 GHz, (b) 1.88 GHz, and (c) 2.35 GHz.
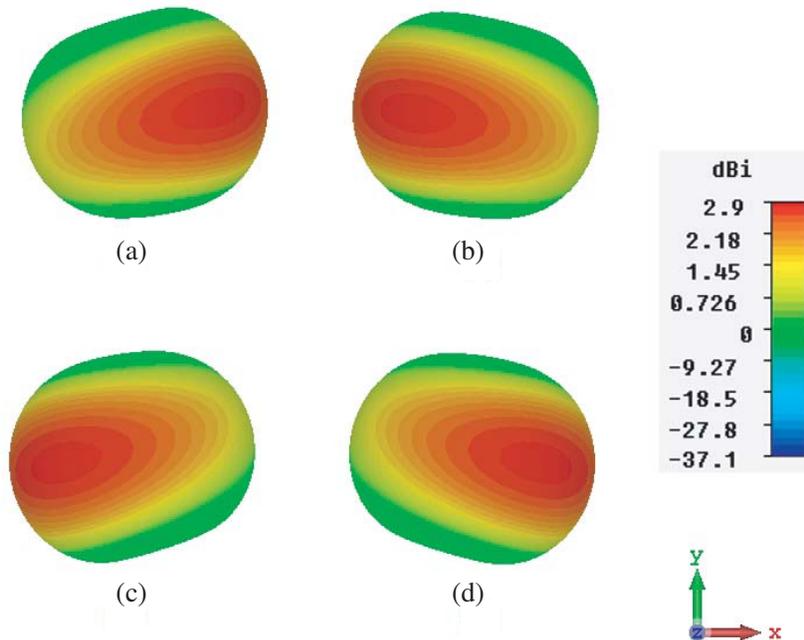
Figure 4. Simulated 3D directive gain radiation patterns of the proposed four-element LHM MIMO antenna array at the lowest resonant mode, 1.39 GHz when (a) port 1 is activated, (b) port 2 is activated, (c) port 3 is activated, and (d) port 4 is activated.

isolation.

Figure 4 displays the simulated 3D directive gain radiation patterns of the proposed four-element LHM MIMO antenna array at the lowest resonant mode of 1.39 GHz when port 1 to port 4 are separately activated (in each case, the other three ports are matched with 50 Ω loads). The figure shows that the antenna radiates toward $-x$-, and $+x$-axis directions when corresponding port is activated. The directive gain values of the lowest (1.39 GHz), middle (1.88 GHz), and highest (2.35 GHz) resonant modes are 2.9, 3.6, and 3.4 dBi, respectively.

Envelop correlation coefficient (ECC) of closely spaced antenna elements is another important parameter besides port isolation used to fairly evaluate the performance of the MIMO antenna. ECC is a measure of the correlation of adjacent antenna elements with each other. Ideally, low ECC (less than 0.5) is required with high port isolation [1].
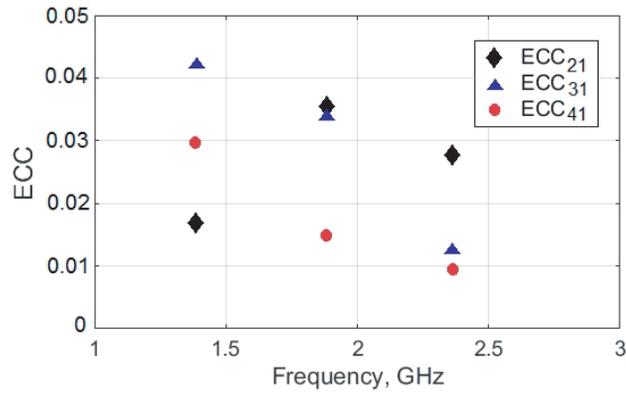
Figure 5. Simulated ECC values versus frequency of the proposed four-element LHM MIMO antenna array.

(a)

(b)
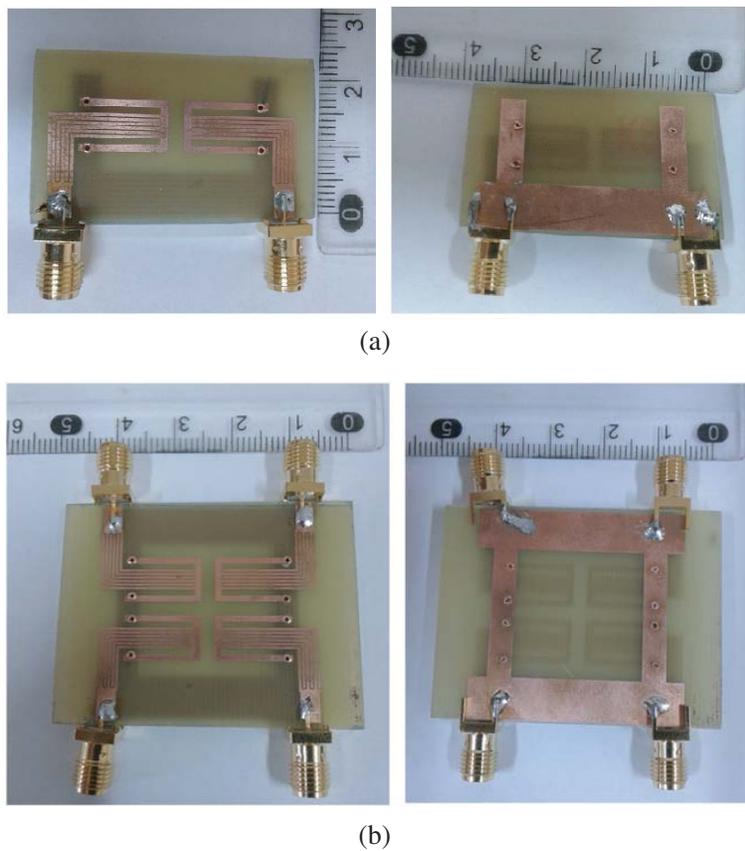
Figure 6. Top- and bottom-view of the fabricated MIMO antenna arrays models. (a) Two-element configuration and (b) four-element configuration.
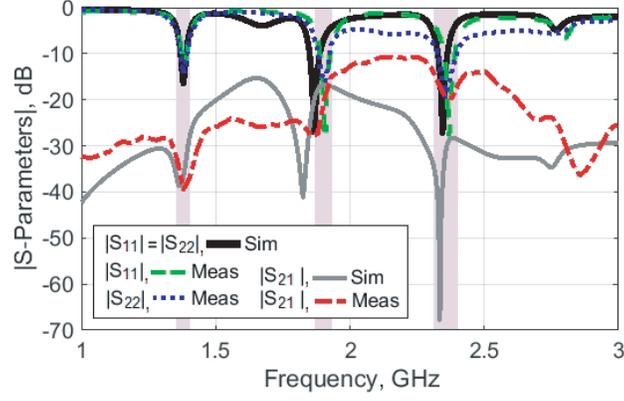
Figure 7. Measured and simulated S-parameters versus frequency of the proposed two-element LHM MIMO antenna array. (The labels assigned for the measured curves).
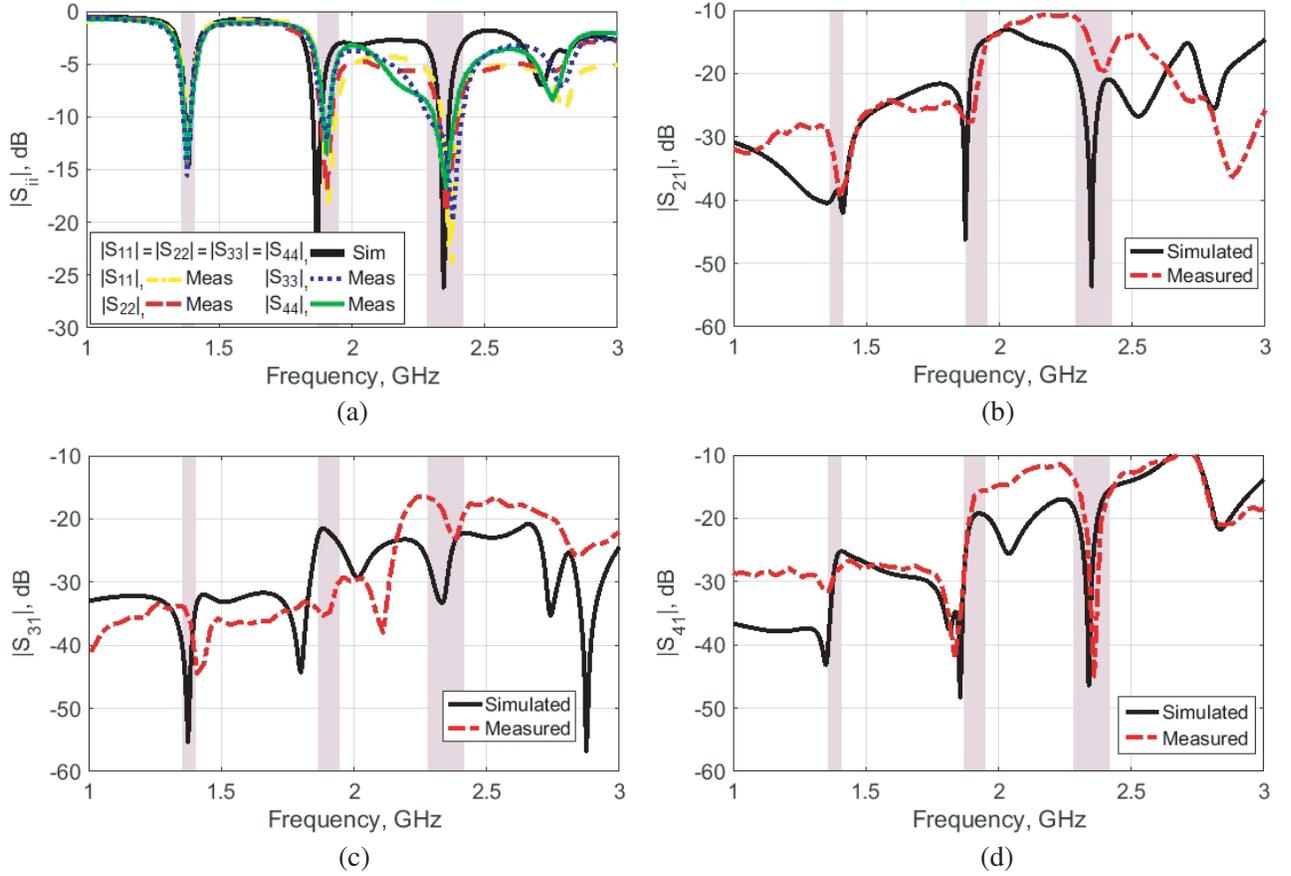
Figure 8. Measured and simulated S-parameters versus frequency of the proposed four-element LHM MIMO antenna array. (a) $|S_{ii}|$, (b) $|S_{21}|$, (c) $|S_{31}|$, and (d) $|S_{41}|$. (The labels assigned for the measured curves).

On the basis of the 3D far-field radiation patterns, the ECC values can be computed as [33]

$$ECC = \frac{\left| \iint_{4\pi} [F_1(\theta, \phi) \cdot F_2(\theta, \phi)] \right|^2}{\iint_{4\pi} |F_1(\theta, \phi)|^2 \, d\Omega \iint_{4\pi} |F_2(\theta, \phi)|^2 \, d\Omega} \tag{1}$$

where $Fi(\theta, \phi)$ is the 3D far-field field radiation pattern when port i is activated.

Normally, different radiation patterns for antenna elements exhibit small ECC values. On the other hand, same radiation patterns exhibit large ECC values. Figure 5 points out that the computed ECC values among all elements of the four-element LHM MIMO antenna at the three operating bands are small and below the threshold value of 0.5, which indicates that the proposed MIMO antenna has low field correlation.

3. EXPERIMENTAL VALIDATION AND DISCUSSION

To validate the simulated results of the designed antenna arrays, prototypes based on optimized dimensions were fabricated using printed circuit board (photolithographic) technology and underwent experimental tests. Pictures of the implemented models are shown in Figure 6. S-parameters of the two antenna array models were measured with the vector network analyzer HP8719ES. Figure 7 shows the measured S-parameters curves of the two-element LHM MIMO antenna array together with simulation ones. The measured and simulated curves shown in Figure 8 are for the LHM MIMO antenna array of four elements. As can be seen in the two figures, the measured and simulated reflection- and transmission-coefficient curves are in good agreement. It can be noticed that the two MIMO antenna configurations have almost same reflection coefficients ($|S_{ii}|$) curves, owing to the symmetry of the array elements. However, the slight discrepancy which appears in the measured curves may be attributed to the antennas fabrication and soldering errors which result in non-identical array elements. For the two-element configuration, results in Figure 7 show that the measured 10 dB impedance bandwidths are 40 MHz (1.37–1.41 GHz, 2.90%) at the center frequency of 1.39 GHz, 50 MHz (1.88–1.93 GHz, 2.62%) at the center frequency of 1.905 GHz, and 70 MHz (2.33–2.40 GHz, 2.96%) at
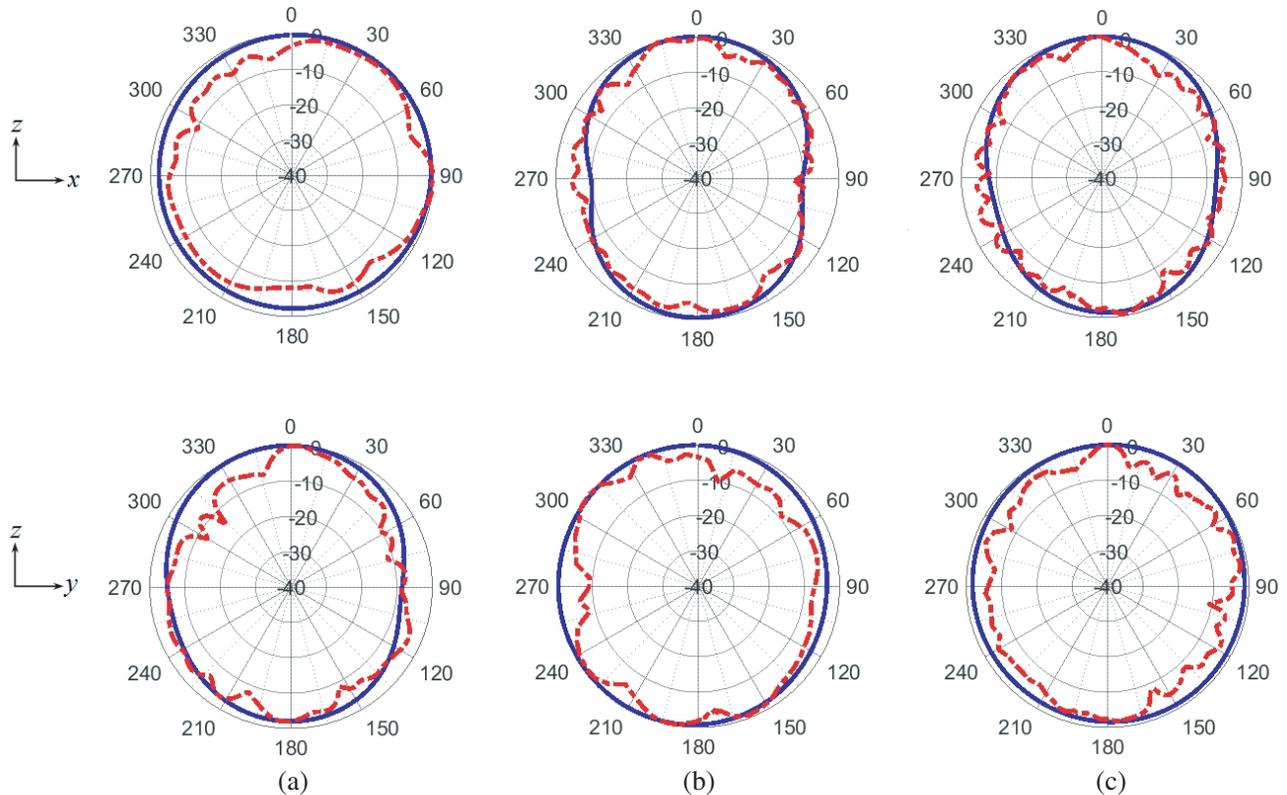
Figure 9. Measured (red dashed line) and simulated (blue solid line) normalized radiation patterns of the proposed four-element LHM MIMO antenna array in the x-z plane (top) and the y-z plane (bottom) when port 1 activated at frequencies (a) 1.39 GHz, (b) 1.88 GHz, and (c) 2.35 GHz.

the center frequency of 2.365 GHz. On the other hand, for the four-element configuration, results in Figure 8 show that the measured 10 dB impedance bandwidths are 40 MHz (1.37–1.41 GHz, 2.90%) at the center frequency of 1.39 GHz, 30 MHz (1.88–1.91 GHz, 1.58%) at the center frequency of 1.895 GHz, and 120 MHz (2.29–2.41 GHz, 5.11%) at the center frequency of 2.35 GHz. These characteristics meet the required bandwidth specifications of Wireless Medical Telemetry Service, WMTS (1.395–1.40 GHz), Digital Enhanced Cordless Telecommunications, DECT (1.88–1.90 GHz), and Wireless Communications Service, WCS (2.345–2.360 GHz) applications. Also, in the two figures, good coupling values can be observed, which ensure that the closely packed array elements of the two MIMO antennas configurations are well isolated. However, the fabricated non-identical array elements models also affected the measured isolation values between the MIMO antennas elements. The worst isolation value was 10.5 dB, which was measured at 2.35 GHz between port 1 and port 2 of the four-element configuration.

The measured and simulated normalized radiation patterns of the proposed four-element LHM MIMO antenna array in x-z ($\phi = 0$) and y-z ($\phi = 90$) planes at 1.39, 1.88, and 2.35 GHz when port 1 is activated are plotted in Figure 9. The radiation patterns when port 2 is activated are plotted in Figure 10. The antenna exhibits radiations with fairly good omnidirectional characteristics at all operating bands in both the planes. The slight ripples observed in the measured curves may be attributed to the EM interference by the environment due to imperfect shielding of the measurement system and some minor imperfections in the Anechoic Chamber.
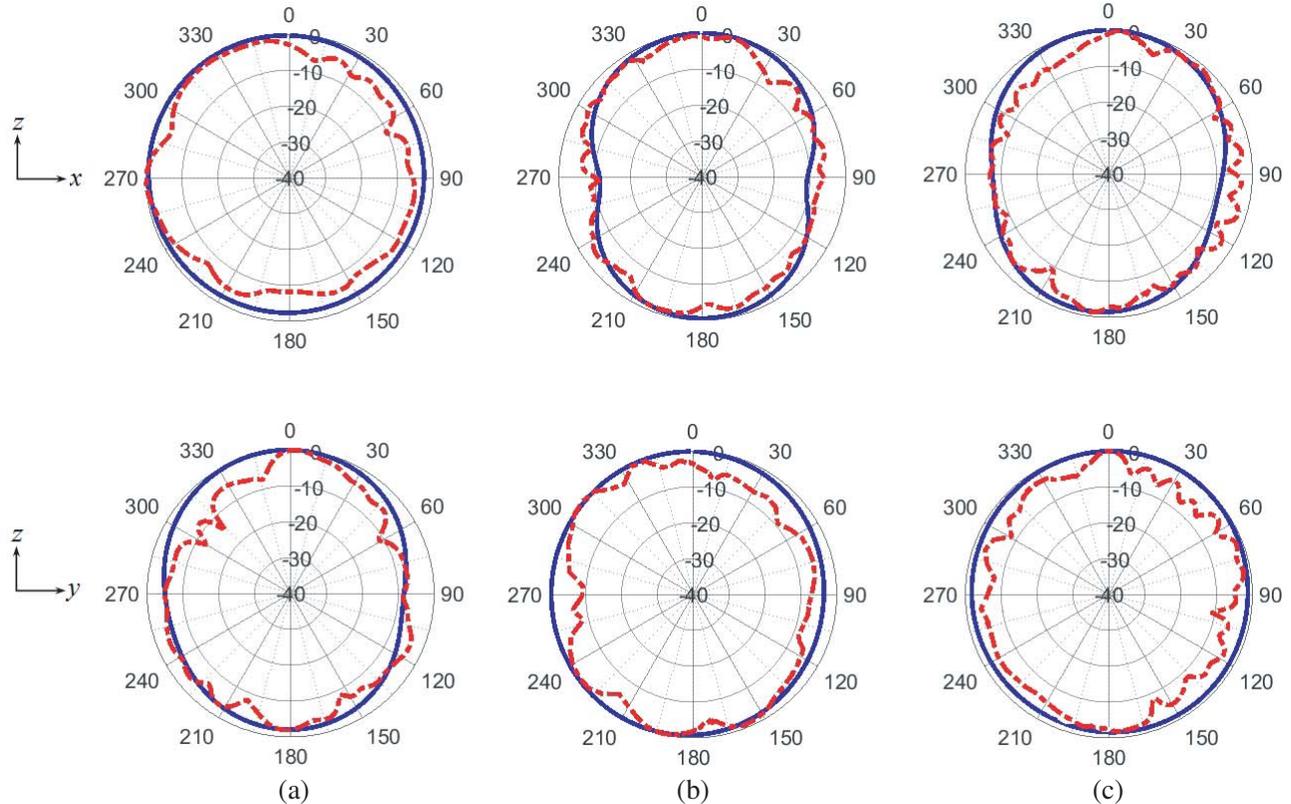
Figure 10. Measured (red dashed line) and simulated (blue solid line) normalized radiation patterns of the proposed four-element LHM MIMO antenna array in the x-z plane (top) and the y-z plane (bottom) when port 2 activated at frequencies (a) 1.39 GHz, (b) 1.88 GHz, and (c) 2.35 GHz.

Table 1 compares the features of the proposed LHM MIMO antenna arrays with other related works. It is clear that the proposed design offers good isolation with compact size. Furthermore, the proposed design features multiband response which can be used for different wireless applications.

Table 1. Comparison between proposed LHM MIMO antenna arrays designs and previous related works.

Ref.	Approach	f_o (GHz)	10 dB-BW (MHz)	Size (mm^2)	No. of elements	Edge-to-edge spacing[a]	Min. isolation (dB)	Max. ECC
[13]	IDC and thin-strip	2.52	110	42×26	2	$0.033\lambda_0$ (4 mm)	18	NA
[14]	Two shunt patches and meandered stubs	2.4	120	44×30	2	$0.06\lambda_0$ (7.5 mm)	35	0.01[b]
[15]	Shunt double-layered ring	1.74	45	50.8×63	2	NA	25	0.05[b]
[16]	IDC and shunt stub	5.8	90	29.3×26	2	$0.034\lambda_0$ (1.8 mm)	35	0.0002[b]
[17]	IDC and two shunt meandered stubs	2.51 3.52 5.76	200 270 1250	45×25	2	$0.04\lambda_0$ (5 mm)	15	0.012[b]
[18]	Spiral resonator	5.1	200	43×36	2	$0.05\lambda_0$ (3.2 mm)	28	NA
This work	Right-angled bend IDC with dual symmetrical shored stubs	1.39 1.88 2.35	20 40 40	35×21 35×35	2 4	$0.0093\lambda_0$ (2 mm)	18	0.042

[a] Calculated at the lower resonance frequency.

[b] ECC values were calculated from S-parameters and this is not completely correct for lossy antennas.

4. CONCLUSION

Two low-profile metamaterial-based MIMO antenna arrays with high port isolation and low field coupling for multiband applications have been presented. The proposed MIMO antenna configurations have two- and four-elements etched on FR-4 substrates of total dimensions of 21×35 mm^2 and 35×35 mm^2, respectively. The MIMO antenna design with the two configurations maintains high port and field isolations with edge-to-edge separation between antenna elements equal to only 2 mm ($0.0093\lambda_0$ at 1.39 GHz) without using extra isolation structures, which are desirable for better MIMO performance. Antenna models were fabricated and experimentally measured, and the validity of the proposed design was verified. Both the simulated results and measured data prove that the proposed antenna arrays are suitable for multiband MIMO applications in portable devices.

REFERENCES

1. Sharawi, M. S., *Printed MIMO Antenna Engineering*, Artech House, Norwood, 2014.

2. Sharawi, M. S., "Current misuses and future prospects for printed multiple-input, multiple-output antenna systems," *IEEE Antennas Propag. Mag.*, Vol. 59, 162–170, 2017.

3. Nadeem, I. and D. O. Choi, "Study on mutual coupling reduction technique for MIMO antennas," *IEEE Access*, Vol. 7, 563–586, 2019.

4. Bilal, M., R. Saleem, H. H. Abbasi, et al., "An FSS-based nonplanar quad-element UWB-MIMO antenna system," *IEEE Antennas Wireless Propag. Lett.*, Vol. 16, 987–990, 2017.

5. Mao, C.-X. and Q.-X. Chu, "Compact coradiator UWB-MIMO antenna with dual polarization," *IEEE Trans. Antennas Propag.*, Vol. 62, No. 9, 4474–4480, 2014.

6. Chen, S.-C., Y.-S. Wang, and S.-J. Chung, "A decoupling technique for increasing the port isolation between two strongly coupled antennas," *IEEE Trans. Antennas Propag.*, Vol. 56, No. 12, 3650–3658, 2008.

7. Xia, R., S. Qu, Q. Jiang, P. Li, and Z. Nie, "An efficient decoupling feeding network for two-element microstrip antenna array," *IEEE Antennas Wireless Propag. Lett.*, Vol. 14, 871–874, 2015.

8. Ou, Y., X. Cai, and K. Qian, "Two-element compact antennas decoupled with a simple neutralization line," *Progress In Electromagnetics Research*, Vol. 65, 63–68, 2017.

9. Jiang, T., T. Jiao, and Y. Li, "Array mutual coupling reduction using L-loading E-shaped electromagnetic band gap structures," *Int. J. Antennas Propag.*, Vol. 2016, 1–9, 2016.

10. Chen, Y. S. and C. P. Chang, "Design of a four-element multiple-input multiple-output antenna for compact long-term evolution small-cell base stations," *IET Microw. Antennas Propag.*, Vol. 10, No. 4, 385–392, 2016.

11. Saad, A. A. R., "Approach for improving inter-element isolation of orthogonally polarised MIMO slot antenna over ultra-wide bandwidth," *Electron. Lett.*, Vol. 54, No. 18, 1062–1064, 2018.

12. Saad, A. A. R. and H. A. Mohamed, "Conceptual design of a compact four-element UWB MIMO slot antenna array," *IET Microw. Antennas Propag.*, Vol. 13, No. 2, 208–215, 2019.

13. Zhu, J., and G. V. Eleftheriades, "A simple approach for reducing mutual coupling in two closely spaced metamaterial-inspired monopole antennas," *IEEE Antennas Wireless Propag.*, Vol. 9, 379–382, 2010.

14. Kiem, N. K., H. N. B. Phuong, Q. N. Hieu, and D. N. Chien, "A novel metamaterial MIMO antenna with high isolation for WLAN applications," *Int. J. Antennas Propag.*, Vol. 2015, 1–9, 2015.

15. Kahng, S., J. Jeon, J. Anguera, and T. Park, "A compact MIMO antenna using CRLH configuration double-layered folded ring radiators with planar mushroom decoupling structure," *IEEE Antennas Propag. Mag.*, Vol. 57, No. 2, 123–130, 2015.

16. Ibrahim, A. A. and M. A. Abdalla, "CRLH MIMO antenna with reversal configuration," *AEÜ — Int. J. Electron. Commun.*, Vol. 70, No. 9, 1134–1141, 2016.

17. Nandi, S. and A. Mohan, "CRLH unit cell loaded tri-band compact MIMO antenna for WLAN/WiMAX applications," *IEEE Antennas Wireless Propag.*, Vol. 16, 1816–1819, 2017.

18. Alqadami, A. S., M. F. Jamlos, P. J. Soh, et al., "Left-handed compact MIMO antenna array based on wire spiral resonator for 5 GHz wireless applications," *Appl. Phys. A*, Vol. 64, 123–127, 2017.

19. Caloz, C. and T. Itoh., *Electromagnetic Metamaterials: Transmission Line Theory and Microwave Applications*, John Wiley & Sons, NJ, 2006.

20. Ibrahim, A. A., A. M. E. Safwat, and H. El-Hennawy, "Triple-band microstrip-fed monopole antenna loaded with CRLH unit cell," *IEEE Antennas Wireless Propag. Lett.*, Vol. 10, 1574–1550, 2011.

21. Zheng, L., X, L. Quan, H. J. Liu, and R. L. Li, "Broadband planar antenna based on CRLH structure for DVB-H and GSM-900 applications," *Electron. Lett.*, Vol. 48, No. 43, 1443–1145, 2012.

22. Ha, J., K. Kwon, Y. Lee, and J. Choi, "Hybrid mode wideband patch antenna loaded with a planar metamaterial unit cell," *IEEE Trans. Antennas Propag.*, Vol. 60, No. 62, 1143–1147, 2012.

23. Li, H. P., G. M. Wang, X. J. Gao, and X. F. Zhang, "Multiband antenna based on loading a CPW-fed monopole with one CRLH-TL unit cell," *Progress In Electromagnetics Research Letters*, Vol. 47, 47–53, 2014.

24. Amani, N., M. Kamyab, A. Jafargholi, et al., "Compact tri-band metamaterial-inspired antenna based on CRLH resonant structures," *Electron. Lett.*, Vol. 50, No. 12, 847–848, 2014.

25. Chen, L. and Y. L. Luo, "Compact filtering antenna using CRLH resonator and defected ground structure," *Electron. Lett.*, Vol. 50, No. 21, 1496–1498, 2014.

26. Sharma, S. K. and R. K. Chaudhary, "A compact zeroth-order resonating wideband antenna with dual-band characteristics," *IEEE Antennas Wireless Propag. Lett.*, Vol. 14, 1670–1673, 2015.

27. Abdalla, M. A. and A. A. Ibrahim, "Multi-band meta-material antenna with asymmetric coplanar strip-fed structure," *IEEE APS/USNC/URSI Int. Symp.*, 631–632, Vancouver, BC, July 2015.

28. Wu, P. C., L. Chen, and Y. L. Luo, "Miniaturised wideband filtering antenna by employing CRLH-TL and simplified feeding structure," *Electron. Lett.*, Vol. 51, No. 7, 548–550, 2015.

29. Li, H., Q. Zheng, J. Ding, and C. Guo, "Dual-band planar antenna loaded with CRLH unit cell for WLAN/WiMAX application," *IET Microw. Antennas Propag.*, Vol. 12, No. 1, 132–136, 2018.

30. Lee, C. J., W. Huang, A. Gummalla, and M. Achour, "Small antennas based on CRLH structures: concept, design, and applications," *IEEE Antennas Propag. Magazine*, Vol. 53, No. 2, 10–25, 2011.

31. Chu, H. B. and H. Shirai, "A compact metamaterial quad-band antenna based on asymmetric E-CRLH unit cells," *Progress In Electromagnetics Research C*, Vol. 81, 171–179, 2018.

32. Saad, A. A. R., "Approach for miniaturisation of planar antenna based on CRLH structure," *Electron. Lett.*, Vol. 55, No. 18, 977–978, 2019.

33. Vaughan, R. G. and J. B. Andersen, "Antenna diversity in mobile communications," *IEEE Trans. Veh. Technol.*, Vol. 36, No. 4, 149–172, 1987.